Supplementary Material for

Reach and grasp by people with tetraplegia using a neurally controlled robotic arm

Leigh R. Hochberg, Daniel Bacher*, Beata Jarosiewicz*, Nicolas Y. Masse*, John D. Simeral*, Joern Vogel*, Sami Haddadin, Jie Liu, Sydney S. Cash, Patrick van der Smagt‡, and John P. Donoghue‡

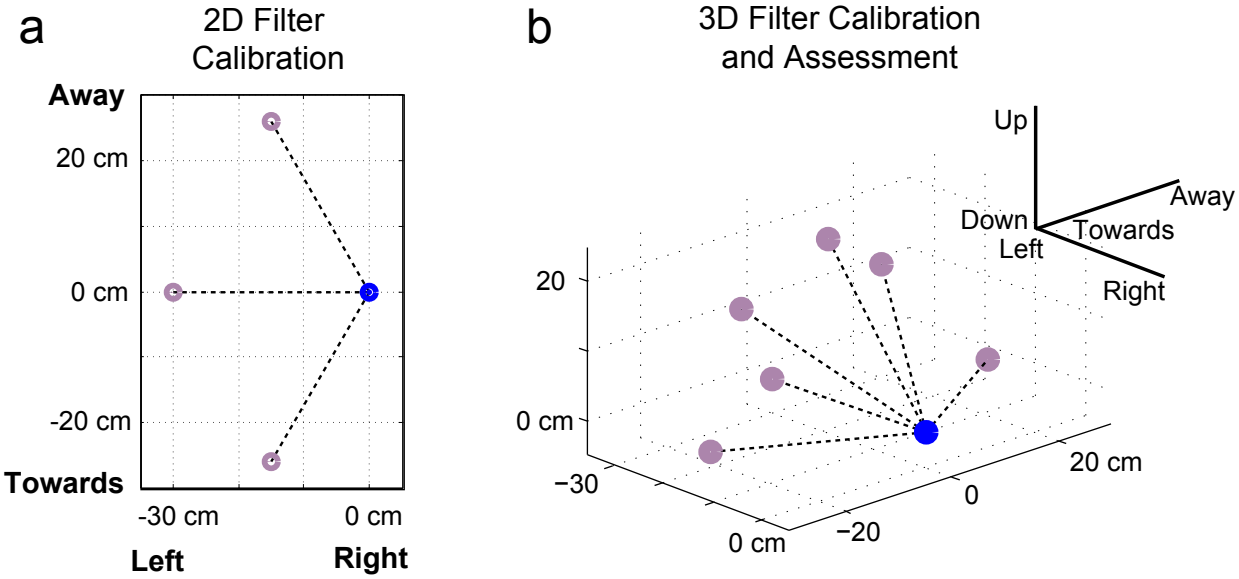

Supplementary Figure 1. Target locations. (**a**) Target locations used to calibrate the 2D filter used for the drinking demonstration. The "home" target (blue circle) location was specified as (0 cm, 0 cm). The centers of the other three targets (purple circles) were located 30 cm away from the home target at (-30 cm, 0 cm), (-15 cm, -26 cm) and (-15 cm, 26 cm). (**b**) Target locations for the 3D filter movement and grasp task. The home target (blue circle) location was specified (in cm) as (0, 0, 0) [left/right,towards/away,down/up]. The other 6 targets (purple circles) were located 30 cm from the home target at (-15, -26, 0), (-22.5, -13, 15), (-30, 0, 0), (-19, 0, 23), (-22.5, 13, 15), and (-15, 26, 0).

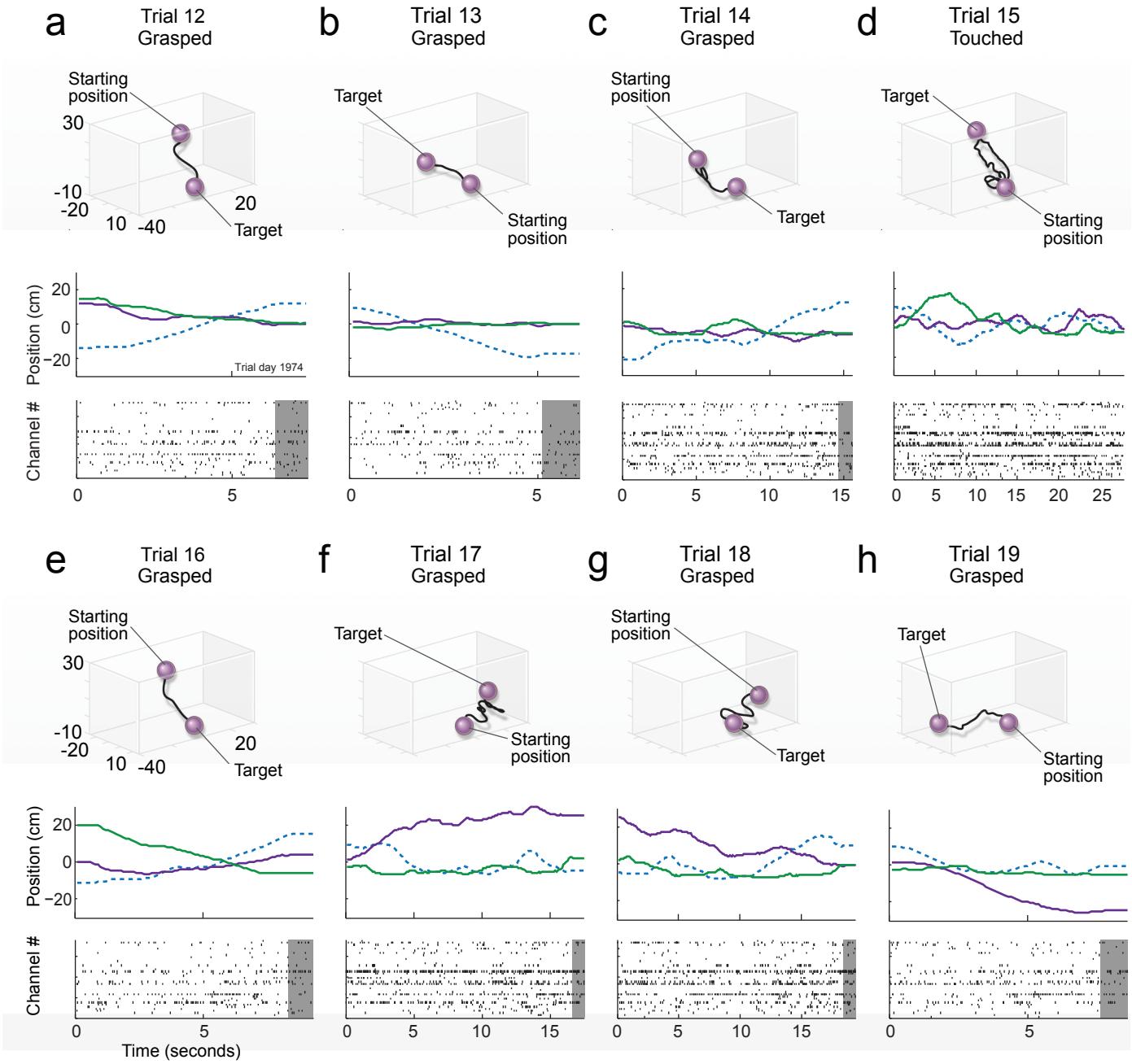

Supplementary Figure 2. Eight consecutive trials from the first DEKA (trial day 1974) session demonstrating some of the 3D neural control achieved in this study. The participant successfully grasped the target in seven of the trials and successfully touched the target with the hand in all eight trials. (**a**) The top panel shows the trajectory from this trial in the 3D environment. The middle panel shows the recorded position of the robot's wrist along the left-to-right axis relative to the participant (dashed blue line), the near-to-far axis (purple line) and the up-down axis (green line). The bottom panel shows the single-trial unit raster from all units used to control prosthetic arm movement. Each row represents the activity recorded at one electrode and each tick represents a threshold crossing (calculated offline). The grey shaded area shows the one second period after the hand was first commanded to grasp. (**b-h**) The same data are shown for the next 7 trials (trial 15 was a successful touch and the rest were successful grasps). These eight trials are also shown in Supplementary Movie 2.

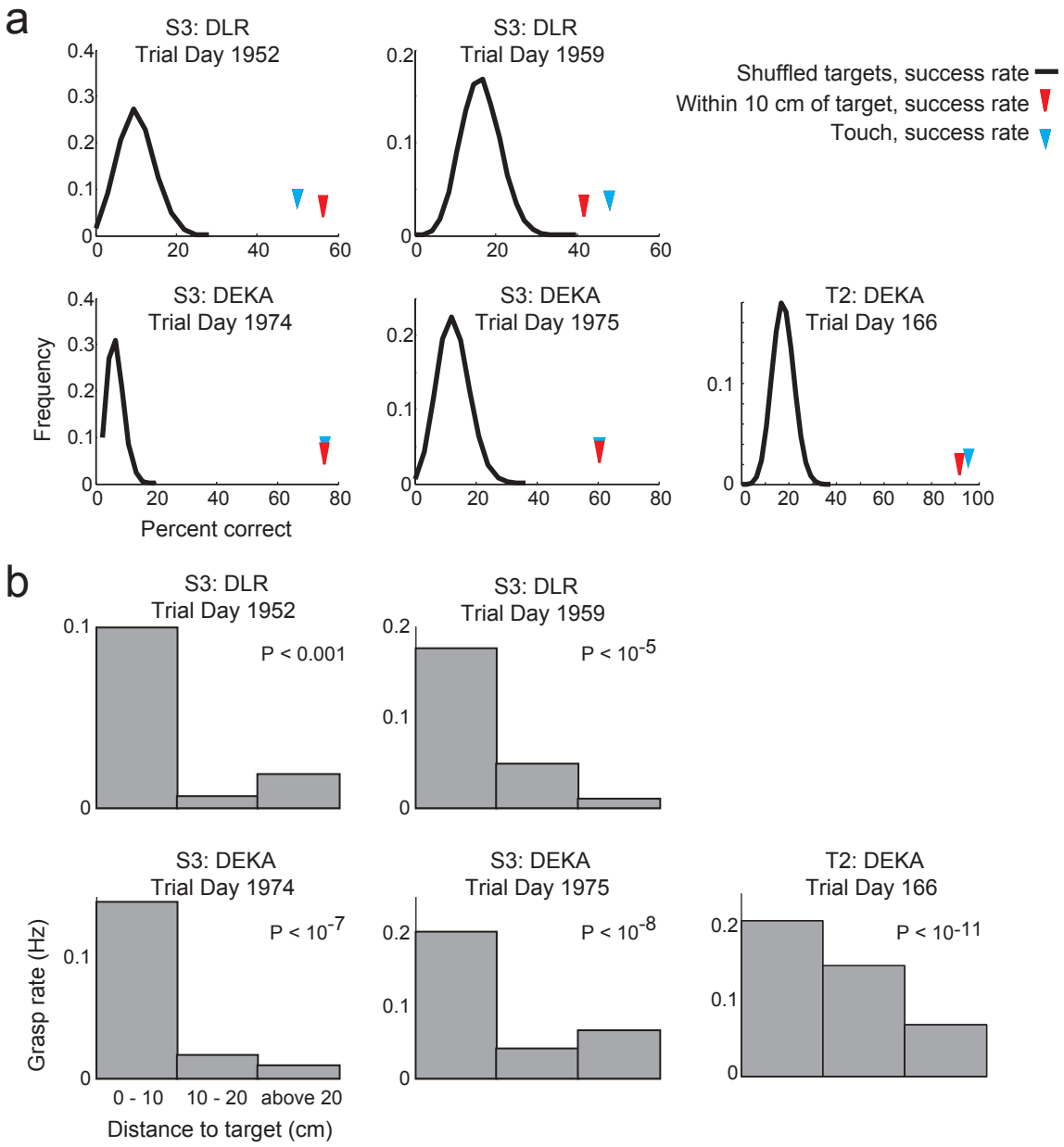

Supplementary Figure 3. Comparing performance to chance levels. (**a**) We performed a bootstrap analysis to test whether the participants' ability to move the robotic hand towards the targets was above chance. We compared the percentage of trials in which the participant brought the endpoint within 10 cm of the target location (red arrow), and the percentage of trials that the participant touched the target (blue arrow), to the bootstrapped distribution showing the percentage of trials the participant would have come within 10 cm of a random target by chance (black curve). Note that since the actual foam-ball target could move if the robotic arm contacted the ball or its supporting rod, it was possible for the participant to touch the target (i.e. to achieve the functionally relevant task of touching the target regardless of how far it may have been displaced by bending the support rod) more often than coming within 10 cm of the initially set target position (e.g. trial day 1959). The bootstrapped distribution was calculated for each session by randomly choosing different targets for each trial and determining whether the actual endpoint trajectory came within 10 cm of the target for each trial, yielding a simulated "success rate". This calculation was repeated 100,000 times. In all five sessions, the true success rates were significantly higher than the bootstrapped success rates for randomly selected targets. (**b**) We also tested whether the participant closed the robotic hand near the target more often than expected by chance. To do this, the grasp rate was calcuated in three bins: when the endpoint was within 10 cm of the target, 10 to 20 cm from the target, and over 20 cm from the target. Grasp rates were greatest when the endpoint was within 10 cm of the target, and the distribution for all five sessions was significantly different from uniform (Chi-square test, p-values shown in insets).

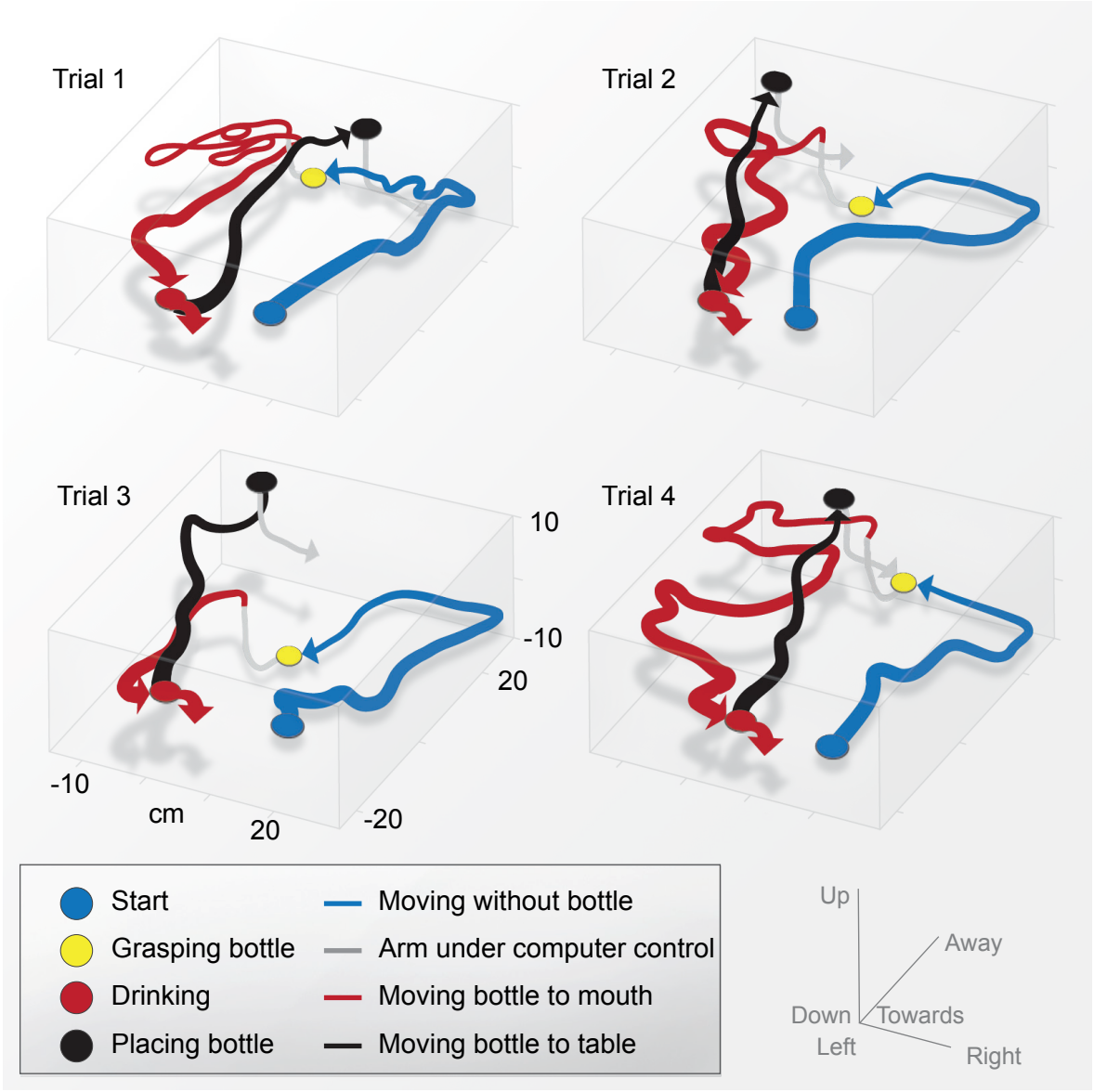

Supplementary Figure 4. Robotic hand trajectories in the successful drinking trials. All four successful trials followed the same sequence: the participant moved the robot hand from the start position to align its opening around the bottle (blue line), grasped the bottle (yellow circle), moved the bottle towards her mouth (red line), drank from the bottle (red circle and curved arrow), and moved the bottle back over the table (black line) before placing it back down (black circle). The grey lines show the vertical movement segments which were under computer control but were initiated by the participant's neurally-controlled state command.

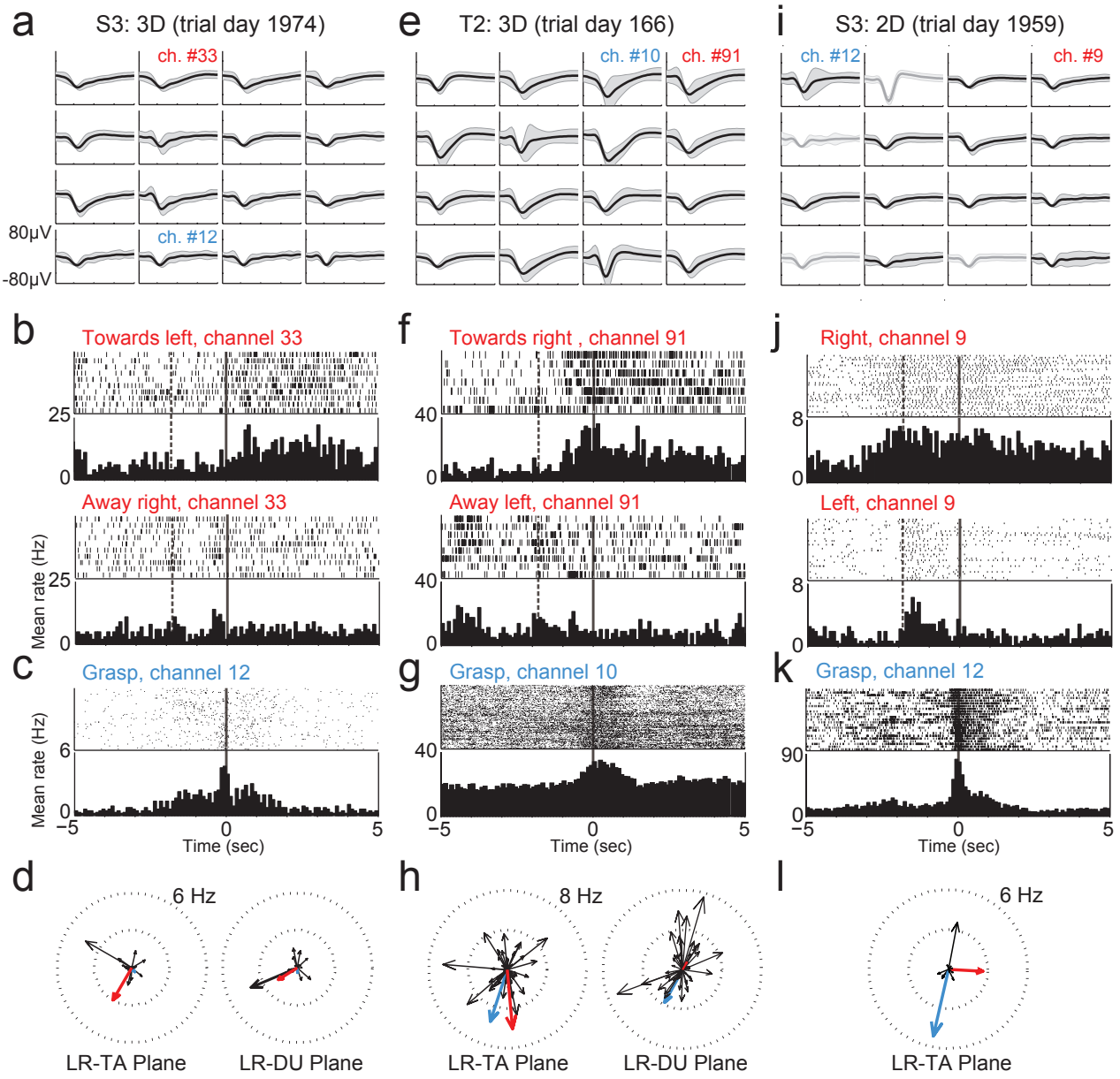

Supplementary Figure 5. Examples of neural signals from three sessions and two participants: a 3D reach and grasp session from S3 (a-d) and T2 (e-h), and the 2D drinking session from S3 (i-l). (a, e, i) Average waveforms (thick black or gray lines) ± 2 standard deviations (grey shadows) from the 16 units with the largest directional modulation of activity from each session. Histograms and accompanying waveforms from Figure 3 (main text) repeated here for clarity. Units included in the Kalman filter are shown in black. Some channels with historically unreliable recording characteristics were explicitly excluded from the Kalman filter (i, four units with gray mean waveforms). (b,f,j) Rasters of threshold crossings showing directional modulation. Each row of tick marks represents a trial, and each tick mark represents a threshold crossing event. The histogram summarizes the average activity across all trials in that direction. Rasters are displayed for arm movements to and from the pair of opposing targets that most closely aligned with the selected units' preferred directions (the selected units are also indicated in the other panels). (b) and (f) include both closed-loop filter calibration trials and assessment trials and (j) includes only filter calibration trials. Time 0 indicates the start of the trial. The dashed vertical line 1.8 seconds before the start of the trial identifies the time when the target for the upcoming trial began to rise. Activity occurring before this time corresponded to the end of the previous trial, which often included a grasp, followed by the lowering of the previous target and the computer moving the hand to the next starting position if it wasn't already there. (c, g, k) Rasters and histograms for units that modulated with intended grasp state. During closed-loop filter calibration trials, the hand automatically closed starting at time 0, cueing the participant to grasp; during assessment trials, the grasp state was decoded at time 0. (legend continued on next page)

(d, h, l) The preferred directions of all units included in the Kalman filter in these sessions. The length of each preferred direction arrow corresponds to that unit's modulation index (see Methods). The red arrows correspond to the units whose rasters are shown in (b,f,j), and the blue arrows correspond to the units whose rasters are shown in (c,g,k). For 3D sessions, these same sets of preferred directions are shown in two different projections (LR: left-right; DU: down-up; TA: toward-away).

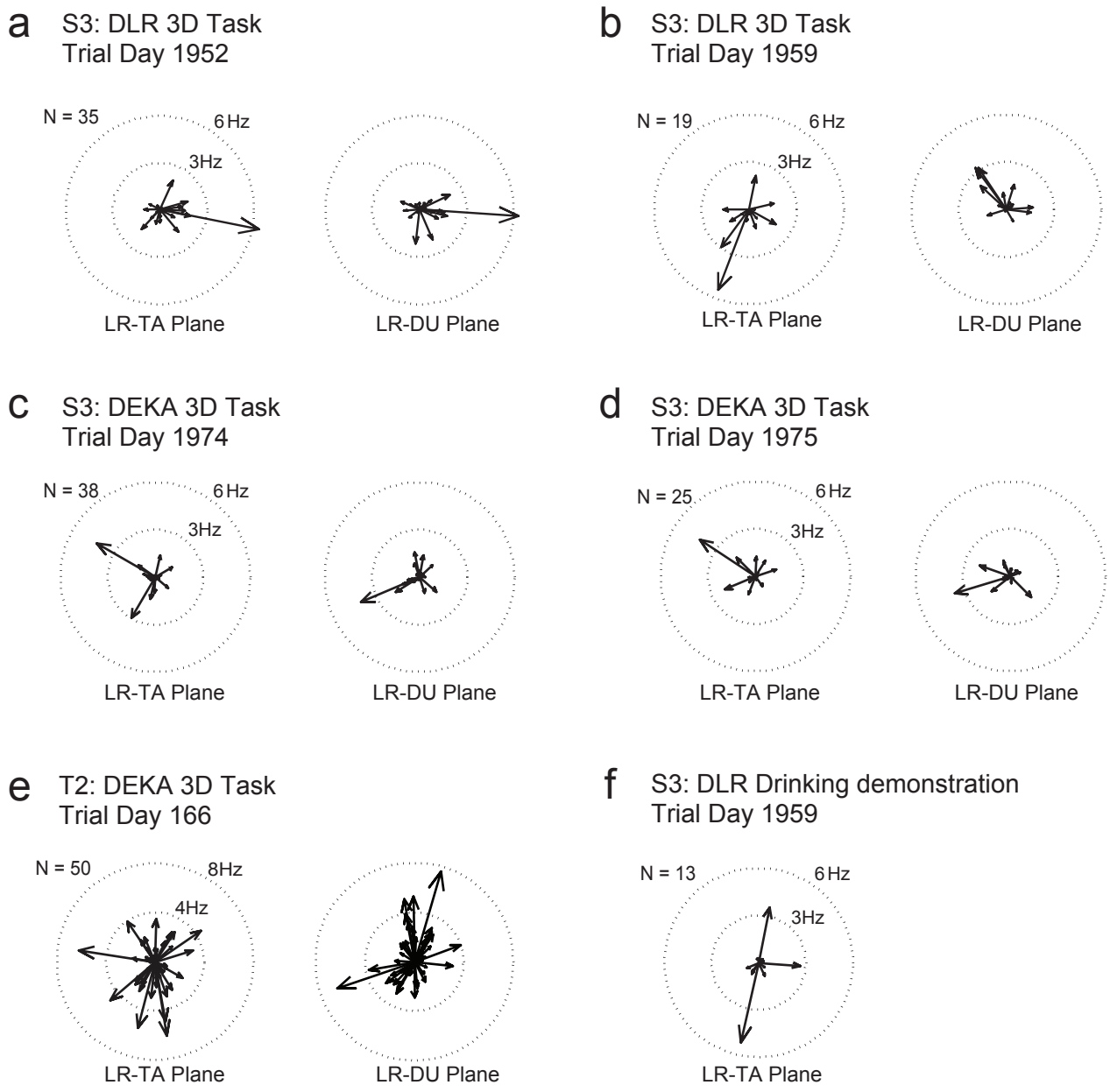

Supplementary Figure 6. Directional tuning for all six sessions. **(a-e)** Each polar plot shows the preferred directions (represented as the angles of the vectors) and the modulation indices (represented as the lengths of the vectors) of all units included in the Kalman filter during each 3D session. The same preferred direction vectors are shown in both the LR-DU and LR-TA planes (LR: left-right; DU: down-up; TA: toward-away). **(f)** Directional tuning for all the units included in the filter for the drinking demonstration. Because control was limited to the tabletop (2D) plane in this task, directional tuning for only the LR-TA plane is shown. Panels c, e, and f are the same as Supple- mentary Figure 5 panels d, h, and l respectively, but are reproduced here to facilitate comparison across all sessions.

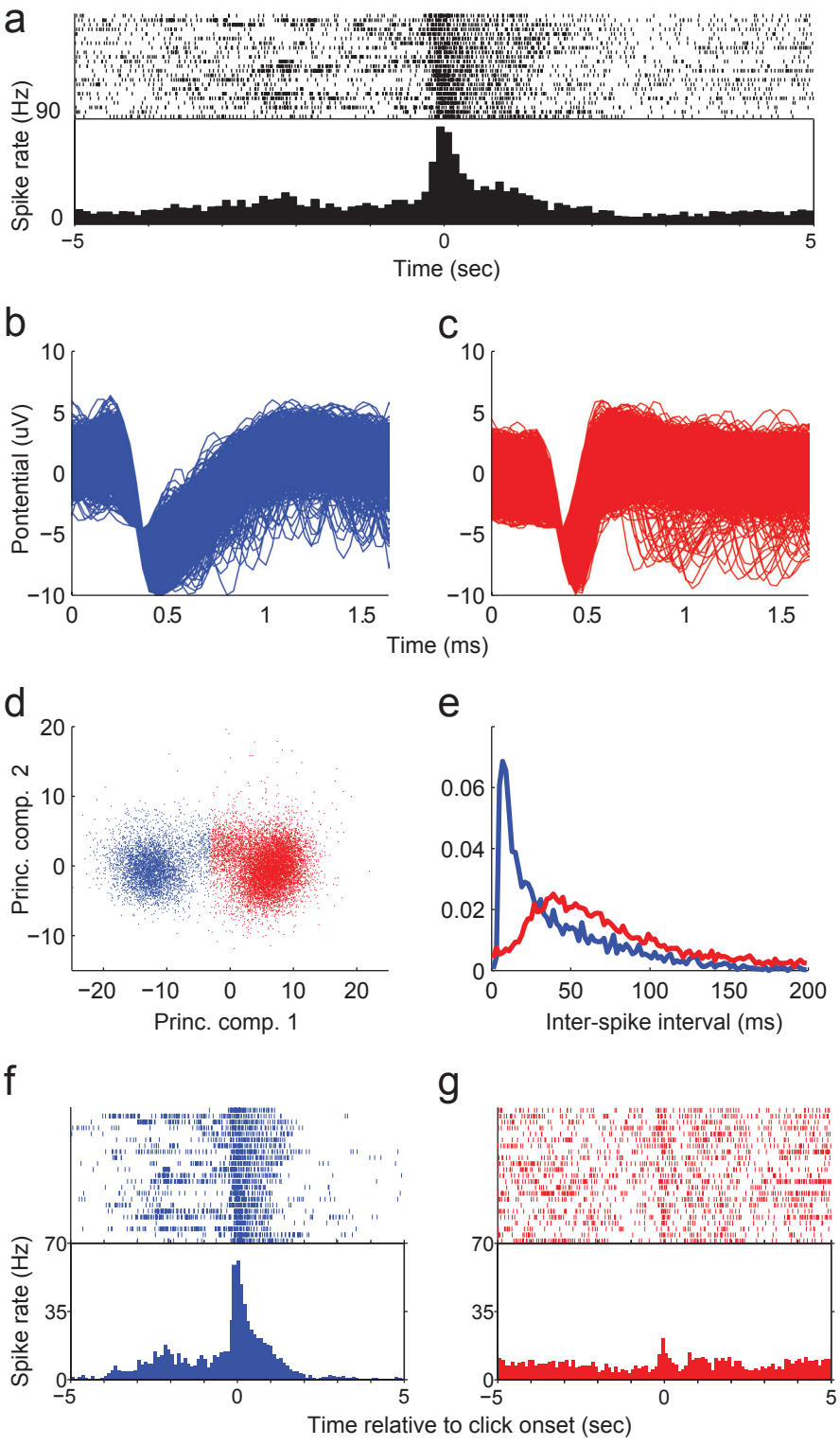

Supplementary Figure 7. Example threshold crossing neural signal contributing to the decoding of a grasp command during the drinking task performed by participant S3. To confirm that the signal that generated the grasp command consisted of spiking neural activity, we examined the symmetrically bandpass-filtered signals of an example channel. (**a**) Raster plot and histogram of the threshold-crossing activity of channel 12 associated with the instruction to grasp (black

vertical line). Each row in the top panels represents a trial and each tick mark represents a threshold crossing event. The histogram summarizes the average activity across all trials involving an instructed grasp command and reveals a rate increase associated with grasp. (**b, c**) Voltage waveforms captured during the threshold-crossing events of channels 12 in (a) could be sorted into two "units" (blue and red) by applying principal component analysis followed by k-means clustering. (**d**) The waveform principal component scores of all threshold crossing events by which waveforms were classified into the units in (b) and (c). (**e**) Inter-spike interval distributions of the sorted units. (**f, g**) The average threshold-crossing rate of the sorted units relative to the instructed grasp command (at time 0) showing that neural activity associated with the blue waveform greatly increased in response to a grasp command whereas the red unit contributed little.

The waveform shape of the blue unit (b) and the shape of its inter-spike interval histogram (e) are consistent with spiking neuronal activity with little or no evidence of confounding noise artefact. This neural activity exhibited reliable grasp-related rate changes (f) that contributed to decoding grasp on this day, whereas the red waveforms demonstrated little grasp-related response and contributed relatively little. Neither unit showed evidence of non-neural artifact associated with grasp. These findings confirm that reliable, robust grasp-related rate changes in the threshold-crossing data could be attributed to identifiable neural activity rather than noise or electrical artifact.

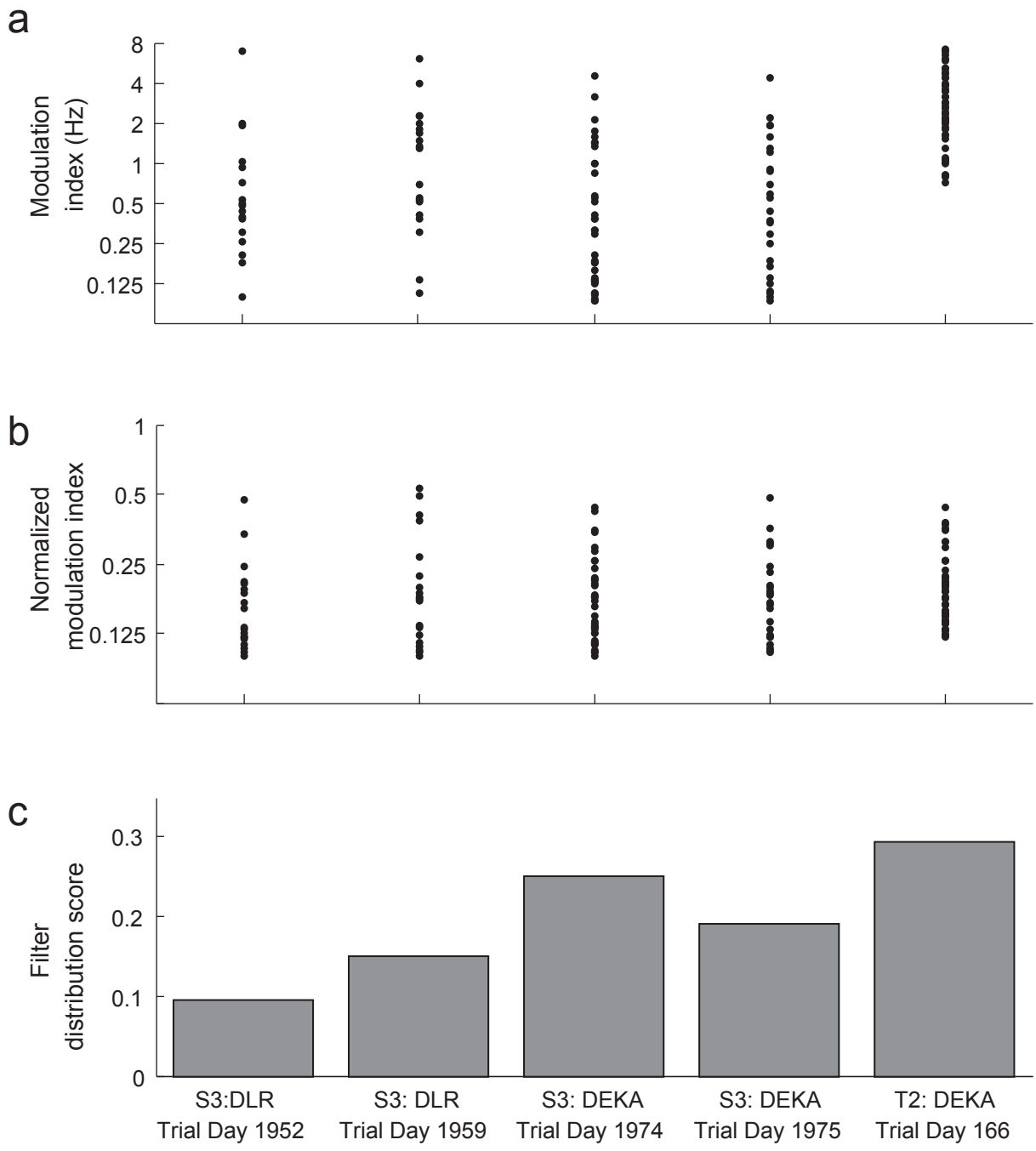

Supplementary Figure 8. Filter properties. **(a)** The distribution of modulation indices from each channel that went into the filters during the five 3D sessions. **(b)** Same as (a), except that the modulation indices are normalized by the standard deviation of the residuals (see Methods). The normalized modulation indices measure a type of tuning quality. **(c)** Filter distribution scores across the five 3D sessions. A score of 1 would indicate that the preferred directions were uniformly distributed in 3D, and a score of 0 indicates that the preferred directions were confined to a 2D plane.

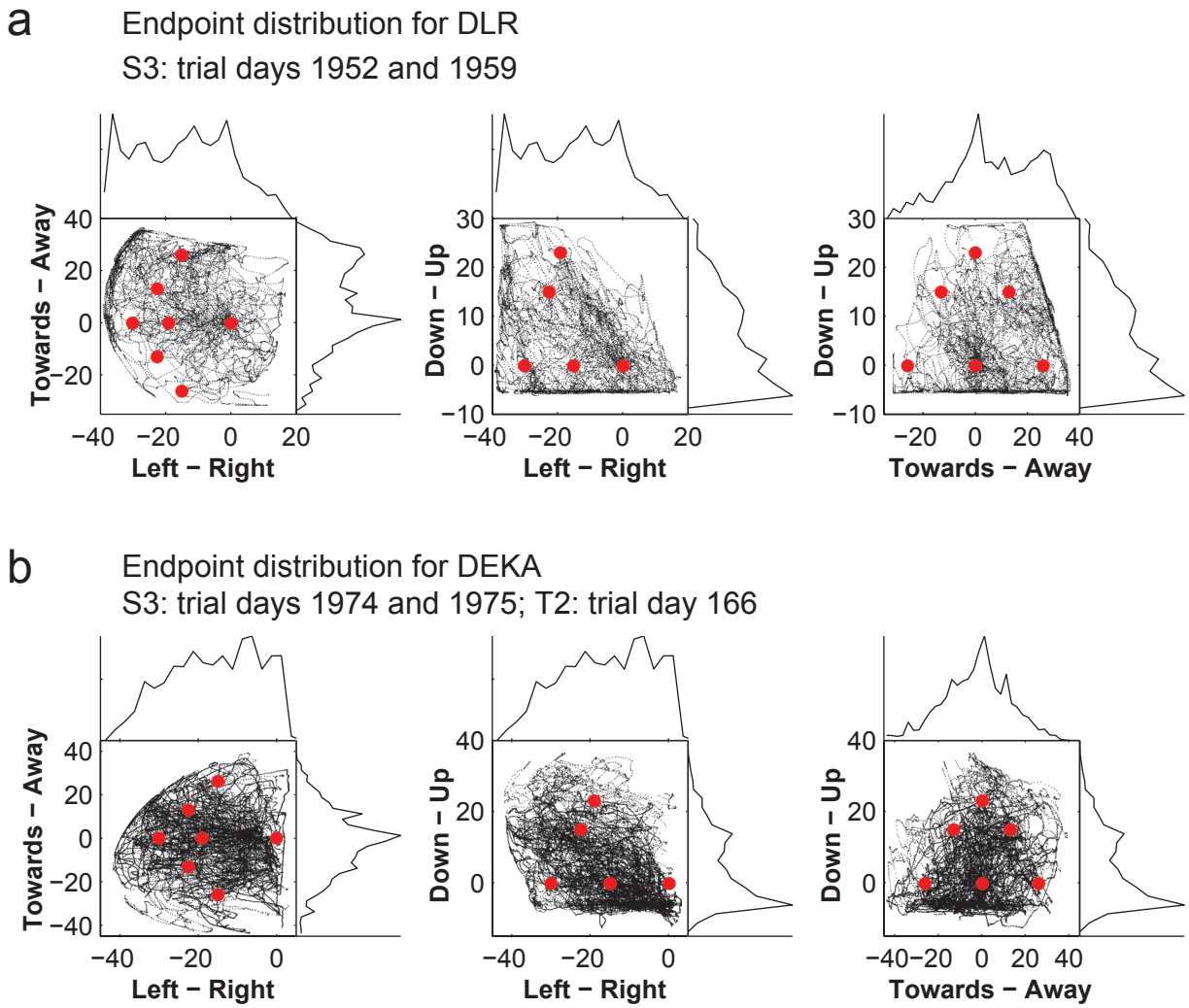

Supplementary Figure 9. Distribution of the endpoint locations of the robotic arm in 3D space. (**a**) The endpoint distribution projected onto the left-right-down-up plane (left panel), the left-right-towards-away plane (middle panel) and the down-up-towards-away plane (right panel) for the two DLR 3D sessions. Black dots represent the endpoint position for each time bin while the red circles give the position of targets. The histograms above and to the right of each panel show the distribution of the endpoint projected onto each axis. (**b**) Same as (a), except for the three DEKA sessions.

Session	Trial Day	Participant	Number of channels included in Kalman Filter	Number of channels included in State Decoder
DLR 3D Task	1952	S3	35	25
DLR 3D Task	1959	S3	19	20
DLR Drinking Task	1959	S3	13	16
DEKA 3D Task	1974	S3	38	18
DEKA 3D Task	1975	S3	25	21
DEKA 3D Task	166	T2	50	50

Supplementary Table 1. For each session: the number of channels included in the Kalman filter used to control the endpoint velocity of robotic arm, and the number of channels included in the state decoder used to control the grasp state of the robotic hand.

Supplementary Discussion

Regarding relative performance of the DLR vs. DEKA sessions

S3's target acquisition and grasp performances were better in the DEKA sessions than in the DLR sessions (Fig 1e). Several factors might have contributed to the performance differences between robot types. First, the aperture of the DLR hand (8 cm) was only slightly (1.3x) larger than the target ball diameter (6 cm), whereas the aperture of the DEKA hand was 1.8x larger (11 cm). Thus, aligning the aperture of the hand with the target required more precision using the DLR robot. Second, shorter trial timeouts were used in the DLR robot sessions: DLR trials had a 20 second timeout (except for 8 trials which had a 30 second timeout), whereas DEKA trials had a 28 second timeout. Third, improvements made to the calibration of the grasp state decoder after the first DLR session (see Methods) may have led to improved grasp control. Fourth, the orientation of the DLR hand was roughly perpendicular to the participant's line of sight, while the DEKA hand was rotated toward the participant, possibly facilitating the alignment of the open part of the hand with the target.

Differences in the depth of directional tuning or the number of tuned units across the neuronal ensemble could be an important determinant of performance; however, the modulation indices of the units included in the filters across these sessions did not appear correlated with performance (Supplementary Fig. 2, 3a,b). Another factor that might affect neural control of the robot arm is the distribution of the units' preferred directions. For example, if all preferred directions were confined to a 2D plane, then the participant would not be able to move the arm in the direction perpendicular to this plane. Thus, we also measured the directional tuning distribution in 3D space to test whether it could be responsible for the differences in performance between the DEKA and DLR sessions. First, we scaled the preferred direction vector of each unit

by its normalized modulation index (see Methods) using the formula $\|H_i\|/\sqrt{Q_{ii}}$, where H_i denotes the row of the Kalman H matrix corresponding to channel i, and the subscript ii denotes the diagonal element of the Q matrix corresponding to the same channel. Then we formed a matrix of these values across all channels, along with their negative copies, and then calculated the three eigenvalues of the matrix, whose relative values give a measure of the amount of tuning in three orthogonal directions. The ratio of the smallest to the largest eigenvalue thus gives a "filter distribution score" which is 1 when directional tuning is isotropic in three dimensions and 0 when the preferred directions are confined to a 2D plane. As shown in Supplementary Fig 8c, scores were greater for the last two sessions (DEKA session #3, trial day 1974: 0.251; DEKA session #4, trial day 1975: 0.190) compared to the first two sessions (DLR session #1, trial day 1952: 0.095; DLR session #2, trial day 1959: 0.149). Thus, this improvement in the distribution of the preferred directions could also have contributed to the better performance during the DEKA sessions than during the DLR sessions.

Regarding further improvements to neural interface systems

There are many opportunities to further improve the function of neural interface systems. Additional dimensions of movement and learning-related changes have been observed in MI which could enhance neuroprosthetic control appear to occur in able-bodied NHPs[9,19,27,38,39,40,41], but it remains to be shown whether these properties are present in people with CNS injury. Further improvement might also be obtained by de-noising the neural signal through dimension reduction[42], incorporating additional sensory feedback[2,43], or extending the Kalman filter by allowing for non-linearities and additional kinematic history[44]. It is likely that neurons do not

statically encode simple kinematics parameters[45,46]; thus, decoders based upon more accurate, dynamic encoding models may also substantially improve control.

Supplementary Movie Legends

Supplementary Movie 1: Neuronal ensemble control of the DLR robot arm and hand for three-dimensional reach and grasp by a woman with tetraplegia (S3), trial day 1959 (April 12, 2011). Two minutes of continuous video shows the participant using the BrainGate system to control three-dimensional movements of the robot's hand and hand grasp. She was instructed to grasp the target. In this video, which represents some of her best neural control of the DLR arm, six targets were presented in sequence. She successfully grasped the target on trials 1,3,4, and 6, but only touched the target (which counted as a target acquisition, but not a grasp) on trials 2 and 5. The researcher in the background releases control of the system at the beginning of each block and is positioned to monitor the participant and robot arm. A small LED, located at the base of the DLR arm, was lit to indicate the brief periods where neural control of the limb was suspended. During this period, which occurred after each trial, the hand endpoint was computer positioned precisely at the software-anticipated target location, which then became the next trial's start position (a method utilized to improve the collection of target path metrics). For clarity, a yellow dot (added to the original video) appears in the lower right corner of the screen whenever the small LED is lit indicating computer-based positioning; the dot is green at all other times, indicating full neural control of the limb.

Supplementary Movie 2: Neuronal ensemble control of the DEKA prosthetic arm and hand by a woman with tetraplegia (S3), trial day 1974 (April 27, 2011). Two minutes and 54 seconds of

continuous video showing the participant using the BrainGate system to control three dimensional movements and hand grasp. In this video, which represents some of the best control displayed of the DEKA arm, eight targets are presented in sequence that the participant was instructed to grasp. She successfully grasped the target on all trials except trial 4, in which she successfully touched but did not grasp the target. The LED is lit to indicate the periods where either (a) neural control of the DEKA arm is suspended, as occurred after each trial, or (b) a grasp state command was decoded and 3D movement of the arm was briefly suspended during the grasping motion. The third trial demonstrates an instance in which she successfully acquired the target, but the system software did not register this correct acquisition because the actual target location was different than the computer's estimate of its location. Therefore, a new target was not presented until the timeout was reached. This trial was nevertheless scored during video review as a successful grasp. A yellow dot (added to the original video) appears in the lower right corner of the screen whenever the small LED is lit; the dot is green at all other times, indicating full neural control of the limb.

Supplementary Movie 3: Neuronal ensemble control of the DEKA prosthetic arm and hand by a gentleman with tetraplegia (T2), trial day 166 (November 22, 2011). Three minutes and 51 seconds of continuous video shows the participant using the BrainGate system to control three-dimensional movements and hand grasp. In this video, which is representative of his control of the DEKA arm, eight targets are presented in sequence that the participant was instructed to grasp. He successfully grasped the target on all trials except for trials 5 and 6, in which he successfully touched but did not grasp the target. The LED is lit to indicate the periods where either (a) neural control of the DEKA arm is suspended, as occurred after each trial, or (b) a

grasp state command was decoded and 3D movement of the arm was briefly suspended during the grasping motion. A yellow dot (added to the original video) appears in the lower right corner of the screen whenever the small LED is lit; the dot is green at all other times, indicating full neural control of the limb.

Supplementary Movie 4: BrainGate-enabled use of an assistive robot by S3 to drink a beverage using neurally-controlled 2-D movement and hand state control of the DLR robot arm, trial day 1959 (April 12, 2011). The video begins with the first successful reach, grasp, drink, and replace trial. Neural control of the movement of the DLR arm is enabled only within the plane of the table. After the participant successfully grasps the bottle under neural control (state command), it is raised directly upward off the table under pre-programmed computer control. 2D neural control, parallel to the tabletop plane, is then resumed. If a grasp command is issued when the arm is in a small subset of the workspace immediately near the participant's mouth, the wrist pronates to allow her to sip from the straw (her usual method of drinking, as she does not have adequate motor control of her mouth to drink directly from a glass). After drinking the coffee, she issues another 'grasp' state command, which supinates the wrist to return the bottle to an upright position, at which point 2D neural control is resumed. When she has positioned the hand back over the table to the desired location, she issues a final grasp command, which lowers the bottle, releases the hand, and then withdraws the arm. After the first successful trial, there were two aborted trials (one due to a technical error by a researcher not preparing the hand to initiate a grasp in response to a proper command, the other due to the potential for pushing the bottle off the table, not shown); this was followed by the second and third successful trials, which occurred in succession. On the third trial, a researcher places his hand near the bottle out of concern that it

might be pushed off the table, but in fact the participant successfully grasps the bottle and then drinks from it. This was followed by an aborted trial due again due to the potential for pushing the bottle off the table (not shown), and then a fourth successful trial. The yellow dot in the lower right corner indicates times when the participant issued a grasp command; the dot remains yellow until 2D control is returned, which was dependent upon the phase of the task. 2D control was returned automatically after the bottle was picked up or placed back down on the table; 2D control was also returned if a grasp command was issued when the participant's prior command was to supinate the hand after having just pronated it to take a drink.

References (continued from main text):

31 Kim, S. P. *et al.* Multi-state decoding of point-and-click control signals from motor cortical activity in a human with tetraplegia. *3rd International IEEE/EMBS Conference on Neural Engineering.* 486-489 (2007).

32 Albu-Schaffer, A. *et al.* Soft Robotics: From torque feedback controlled light-weight robots to intrinsically compliant systmes. *Robotics and Automation Magazine: Special Issue on Adaptable Compliance / Variable Stiffness for Robotic Applications* **15**, 20-30 (2008).

33 Liu, H. *et al. IEEE/RSJ International Conference on*in *Intelligent Robots and Systems.* 3692-3697 (2008).

34 Haddadin, S., Albu-Schaeffer, A. & Hirzinger, G. Requirements for Safe Robots: Measurements, Analysis and New Insights. *The International Journal of Robotics Research* **28**, 1507-1527 (2009).

35 Quian Quiroga, R. What is the real shape of extracellular spikes? *Journal of Neuroscience Methods* **177**, 194-198 (2009).

36 Malik, W. Q., Truccolo, W., Brown, E. N. & Hochberg, L. R. Efficient decoding with steady-state Kalman filter in neural interface systems. IEEE Trans Neural Syst Rehabil Eng 19, 25-34 (2011).

37 Taylor, D. M., Tillery, S. I. & Schwartz, A. B. Direct cortical control of 3D neuroprosthetic devices. *Science* **296**, 1829-1832 (2002).

38 Jarosiewicz, B. *et al.* Functional network reorganization during learning in a brain-computer interface paradigm. *Proceedings of the National Academy of Sciences of the United States of America* **105**, 19486-19491 (2008).

39 Saleh, M., Takahashi, K., Amit, Y. & Hatsopoulos, N. G. Encoding of Coordinated Grasp Trajectories in Primary Motor Cortex. *J Neurosci* **30**, 17079-17090 (2010).

40 Humphrey, D. R., Schmidt, E. M. & Thompson, W. D. Predicting measures of motor performance from multiple cortical spike trains. *Science* 170, 758-762 (1970).

41 Ganguly, K. & Carmena, J. M. Emergence of a Stable Cortical Map for Neuroprosthetic Control. *PLOS Biology* 7 (2009).

42 Yu, B. M. et al. Gaussian-process factor analysis for low-dimensional single-trial analysis of neural population activity. *J Neurophysiol* 102, 614-635 (2009).

43 Suminski, A. J., Tkach, D. C., Fagg, A. H. & Hatsopoulos, N. G. Incorporating feedback from multiple sensory modalities enhances brain-machine interface control. *J Neurosci* 30, 16777-16787 (2010).
44 Li, Z. et al. Unscented Kalman Filter for Brain-Machine Interfaces. *PLOS One* 4, (2009).
45 Hatsopoulos, N. G., Xu, Q. Q. & Amit, Y. Encoding of movement fragments in the motor cortex. *J Neurosci* 27, 5105-5114 (2007).
46 Scott, S. H. Inconvenient Truths about neural processing in primary motor cortex. *J Physiol - London* 586, 1217-1224 (2008).